A Distributed Coordination Strategy for Heterogeneous Building Flexible Thermal Loads in Responding to Smart Grids

Zhuang Zheng, *member, IEEE*, Rui Tang, Xiaowei Luo, Hangxin Li, Shengwei Wang

***Abstract*—Air conditioning systems are promising energy flexibility resources for smart grids. However, buildings with various thermodynamics must be coordinated to utilize limited energy flexibility effectively. This study proposes a distributed coordination strategy to coordinate building flexible thermal loads of different characteristics for optimized utilization of energy flexibility in a scalable and distributed manner. It consists of two components:1) an average consensus-based distributed sensing scheme to estimate the average thermal state of charge (SoC) of multiple zones, and 2) a weighted consensus-based distributed allocation module to allocate the demand response (DR) tasks or limited energy resources to multiple zones, proportional to their thermal storage capacities and deviations to the average thermal SoCs. Both algorithms achieve their goals respectively by fully distributed means through a sparse network with neighbor-to-neighbor communication. The sufficient condition for converging the weighted consensus algorithm is also derived for the first time. The proposed strategy is adopted for 1) weighted DR participation of residential inverter air conditioners and 2) weighted water flow redistribution of the commercial building water heating systems under urgent DR events. Simulation results show that adopting the distributed coordination strategy avoids the early depletion of demand flexibility resources and nonuniform thermal comfort sacrifices under uncoordinated control.**

***Index Terms*—smart grid, building flexible thermal loads, heterogeneous capacities and dynamics, average consensus, weighted consensus, distributed coordination**

I. Introduction

As a significant electricity end-use, air conditioning systems are promising demand-side energy flexibility resources for smart grid and renewable energy integration [1], [2]. However, buildings may have different indoor air volumes, structures, materials, internal activities, and external weather disturbances [3]–[5]. These factors result in various thermal storage capacities and thermal dynamics of buildings, which must be appropriately coordinated to achieve optimized utilization of limited building energy flexibility resources. For example, an office building may have multiple thermal zones of different functions, spaces, and materials. The zones with higher thermal inertia should be prioritized in a DR event for uniform thermal comfort sacrifices. The SoCs of multiple distributed battery storage systems should be balanced to avoid the batteries' early dropout in a DR event when the SoCs exceed the limits [6]. The uncoordinated control of demand flexibility (DF) resources with different capacities and dynamics may induce ununiform comfort sacrifices and the early depletion of DF resources [7]. The existing coordination strategies of the heterogeneous building flexible thermal loads can be categorized into centralized and distributed approaches.

The centralized approaches, including central optimization-based [8]–[10] and central rule-based control [6], [11]–[14], calculate control actions with the relevant information about the networks and components and send back individual commands through a star communication network. Jiang et al. [8] developed a central building-to-grid (B2G) optimization model to reduce grid loss and increase the voltage magnitude through the flexible operation of air conditioners. Fontenot et al. [9] proposed a centralized model predictive control (MPC) for coordinated voltage regulation and energy management by integrating buildings, PV inverters, and batteries into the power distribution network and jointly optimizing all components. Zheng et al. [10] proposed a central MPC to coordinate multiple thermal appliances for household peak shaving. Vivian et al. [14] developed a centralized optimization model to coordinate heat pumps for residential peak load shaving that accounts for space heating and domestic hot water demand. Though optimized control actions can be derived, the above central optimization-based approaches rely on centric communication networks with poor scalability and a high information requirement on end-user devices and may face a high computational burden that increases with problem size.

Central rule-based coordination approaches have less computational complexity and data requirement. Lu et al. [11] proposed a temperature priority control (TPC) to coordinate building thermal loads for continuous regulation reserves by a central controller. The central controller collects the state information of each air conditioner in the network and selects air conditioners to be turned on/off based on the difference between real-time indoor temperatures and user setpoints. The TPC method was further modified for commercial buildings' peak load reduction [15], fast primary frequency regulation [16], and load shaping [17]. Jin et al. [12] proposed a coordination strategy by evaluating the relative thermal comfort sacrifices and adjusting the indoor air temperature setpoints stepwise to achieve a uniform indoor temperature rise of all zones during urgent DR events. Tang et al. [6] proposed an adaptive chilled water flow redistribution scheme to deal with

Zhuang Zheng, Hangxin Li and Shengwei Wang *(Corresponding author, email: beswwang@polyu.edu.hk)* are with the Department of Building Environment and Energy Engineering, The Hong Kong Polytechnic University, Hung Hom, Hong Kong

Rui Tang is with the Institute for Environment Design and Engineering, University College London, London, UK

Xiaowei Luo is with the Department of Architecture and Civil Engineering, City University of Hong Kong, Kowloon Tong, Hong Kong

the disordered water flow in commercial water cooling systems in urgent DR events by continually updating the user utility function. Song et al. [13] broadcasted the price adjustments by the microgrid operators to coordinate the air conditioners for eliminating the adverse impact of wind generation variabilities. However, the above online updating processes of the user utility function, indoor air temperature setpoints, and microgrid energy prices are challenging to determine the parameters and face response delay issues [18]. Though the central rule-based control methods are very effective, their performance and reliability depend on costly fast communication links.

Distributed control strategies, relying on limited communication links for sharing data among neighboring agents, have gained popularity for building thermal energy management due to the plug-and-play feature and the robustness to communication link failures. Depending on the decision-making approach, the control strategies are divided into two categories: distributed optimization and distributed rule-based control. Distributed optimization is promising to relieve the computational burden and users' privacy concerns of central optimization-based approaches, i.e., the alternating direction method of multipliers (ADMM) algorithm. Kou et al. [19] decomposed the original centralized optimization problem to utility-level and house-level problems with the ADMM algorithm to coordinate residential demand-side resources at scale and protect the customers' privacy. Li et al. [20] adopted the ADMM algorithm for distributed optimal control of multi-zone air conditioning systems by reformulating the central optimization problem into multiple sub-problems that can be processed in corresponding agents. However, these ADMM applications still require a central coordinator for information exchanges between hierarchical layers. Though fully distributed ADMM algorithms with multi-agent communication topologies are being developed [21], [22], there is a minimal application to building automation and smart grid demand response.

Distributed rule-based control strategies avoid installing long-distance fast communication channels between the central station and the massive number of local controllers at the cost of an increased computational burden than central rule-based control strategies due to the iterative process. Meng et al. [23] developed a consensus-driven distributed control approach to coordinate multiple groups of aggregated building thermal storages to manage network loading by sharing the required real power curtailment among aggregators. Wang et al. [24] also developed a two-level distributed control strategy to share active power adjustments among air conditioner aggregators for distribution network voltage and loading management. However, the above only weighted the DR task allocations among a few aggregators by their maximum amount of active power that each aggregator can adjust. They ignored the real-time thermal dynamics of individual ACs and the scalability of multiple aggregators. Our previous work proposed a distributed temperature priority control of air conditioner clusters for electricity distribution network voltage regulation by estimating the air conditioners' relative cooling priorities based on an average consensus algorithm [2]. Though the real-time thermal dynamics of zones are inferred in a distributed way, the DR tasks are still allocated among aggregators in a centralized way. Zhang et al. [25] proposed a consensus control strategy for inverter air conditioners to share the adjusted temperature interval ratios for renewable energy integration. Though real-time thermal dynamics are considered, the different thermal storage capacities of zones are not considered, and the overall network state information cannot be monitored. More importantly, we found that the weighted consensus algorithm cannot converge under some cases dependent on the selection of weight parameters. However, none of the above works discussed the sufficient condition for converging the weighted consensus algorithm.

Aiming at these shortcomings, we develop a fully distributed rule-based coordination strategy for effectively utilizing the limited building flexible thermal loads with different capacities and dynamics in responding to the smart grid. The proposed coordination strategy is adopted in two case studies for illustration, i.e., the residential inverter air conditioners and the commercial primary constant-secondary variable building water heating system in urgent DR events. The original contributions of this study include:

1) We identify the problems of uneven thermal sacrifice and early depletion of demand flexibility resources when engaging heterogenous residential and commercial building flexible thermal loads for demand response (DR) without coordination, and propose a novel fully distributed rule-based coordination approach that allocates the DR tasks or limited energy resources to multiple building thermal zones by weighting their thermal storage capacities and dynamics;
2) We develop an average consensus-based distributed sensing scheme to estimate the average thermal state of charge (SoC) for dispersed thermal zones through neighbor-to-neighbor communications in the network; A weighted consensus-based distributed allocation method of building thermal energy flexibility is also developed by weighting the thermal storage capacity and the deviations of real-time thermal SoCs to the estimated average thermal SoCs;
3) We derive the sufficient condition for the first time to guarantee the convergence of the weighted consensus algorithm. Numerical experiments validate the effectiveness of the sufficient condition for converging the weighted consensus algorithm and the scalability of the proposed distributed coordination approach when the communication typologies are appropriately selected and the number of connected agents is reasonable. The convergence rate of the average consensus-based distributed sensing scheme is analyzed and compared with the ADMM-based method indicating the consensus-based and ADMM-based distributed controls may have their computational competitiveness under different situations;

II. Building Flexible Thermal Loads for Smart Grid Demand Response

A. Relationship between electric and heat energy of building flexible thermal loads

Building thermal energy flexibility for power supply-demand balance is a low-cost and effective means for deep integration of renewable energy sources in the electric power system. To fully use the heterogeneous building flexible thermal loads for smart grid demand response without sacrificing

the occupant comfort, it is necessary to understand the relationships between electric and heat energy of typical building flexible thermal loads, as summarized in Table I.

TABLE I: Relationship between electric and heat energy of building flexible thermal loads in responding to smart grid

	Residential inverter air conditioners (IACs)	**Commercial primary constant-secondary variable building water heating system**
Heat energy	The cooling supply of IAC changes with the inverter frequency adjustment, inducing indoor temperature variations.	The heating supply suddenly reduces, inducing thermal zones competing for the limited heat water
Coupling equations	$P^t_{IAC} = k_1 u^t_{IAC} + l_1$ $Q^t_{IAC} = -\left(k_2 u^t_{IAC} + l_2\right)$ $T^t_{air} = F_1\left(Q^t_{IAC}, U_{a/m}, C_{a/m}, Q^t_{solar/internal}, T^t_{outdoor}\right)$ where P^t_{IAC} and u^t_{IAC} are the electric power and inverter frequency of the air conditioner, Q^t_{IAC} is the cooling output supplied to the zone, and F_1 is the dynamic thermal model of the zone [26], [27].	$P_{hp} = n \cdot P^k_{hp}$ $Q_{sup} = \sum P^k_{hp} \cdot COP^k = M_{w,pri} \cdot c_\rho \cdot \Delta T_{w,pri}$ $Q_{dem} = \sum M^i_{w,sec} \cdot c_\rho \cdot \Delta T^i_{w,sec}$ $T_{air,i} = F_2\left(Q_{dem,i}, U_{a/m}, C_{a/m}, Q_{solar/internal}, T_{outdoor}\right)$ where P^k_{hp} is the electric power of k^{th} heat pumps, $M_{w,pri/sec}$ are the heat water flow rates of the primary or secondary sides, and F_2 is the dynamic thermal model of the zone [28], [29].
Electric energy	Operating electric power changes with smart grid signals by adjusting the inverter frequency of air conditioners.	Directly shut down some heat pumps during urgent smart grid demand response periods.

B. Conventional uncoordinated control of building flexible thermal loads for smart grid and associated problems

The heterogeneous building flexible thermal loads characterized by different thermal parameters may have diverse thermal dynamics in responding to smart grid demand response signals when adopting conventional uncoordinated control strategies.

For residential inverter air conditioners (IACs), when the DR tasks were evenly allocated to the zones of different characteristics without coordination, it led to non-uniform thermal sacrifices. Fig. 1a shows the simulated indoor temperatures of four residential houses with IACs operating in cooling mode and responding to the load increment signals from 11:00 to 14:00 am. The thermal comfort of zones with small thermal storage capacities will be sacrificed more. Fig. 1b shows the thermal SoC profiles of four zones, and the thermal 'SoC' is defined later in (2). It is observed that the thermal flexibility of zone-1 is depleted in the middle of the DR period due to violations of the lower temperature limit.

For commercial building HVAC systems, directly shutting down some chillers or heap pumps can achieve immediate demand reduction for peak shaving. However, it leads to the disorder of the original air conditioning system and uneven heat distribution among the spaces. Fig. 2 shows the simulated water flow rates and associated temperature variations for a primary constant-secondary variable building water heating system in a cold area by shutting half of the heat pumps for

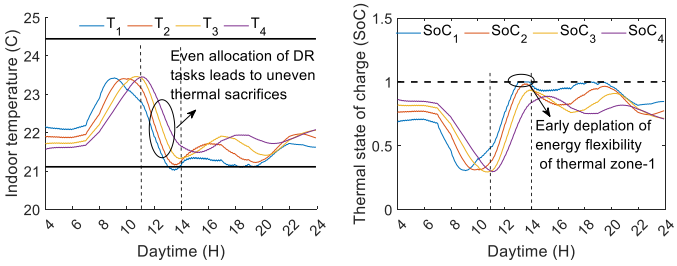

(a) (b)

Fig. 1: Unfair thermal sacrifices and early depletion of demand flexibility of IACs by even DR tasks allocation (a) indoor air temperature and (b) thermal SoC profiles.

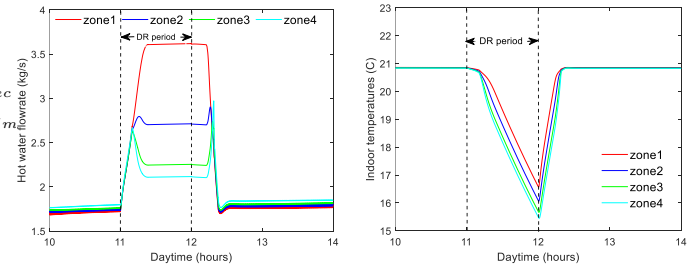

(a) (b)

Fig. 2: Uncoordinated control of building water heating system in a fast DR event (a) heat water flow rate of four zones and (b) indoor air temperature profiles

peak limiting between 11:00 am and 12:00 am. It is observed in Fig. 2a that during the DR event, the hot water distributed to all zones increased significantly due to the valves of radiators being fully open to compete for the limited heating supply after half of the operating heat pumps were shut down. The nearest zone (zone-1) obtained the highest water flow, and the remotest zone (zone-4) obtained the least. Consequently, the indoor temperature decreases of individual zones would be non-uniform (indoor air temperature setpoints of all zones are 21°C), as shown in Fig. 2b. The indoor temperature of zone-4 would reach below 16°C, and the largest temperature difference among zones was about 1.5°C.

To avoid the early depletion of building energy flexibility and the non-uniform thermal sacrifices of uncoordinated control, we develop a novel distributed control strategy for coordinating the heterogeneous building flexible thermal loads with different capacities and dynamics in Section III.

III. Proposed Distributed Coordination Strategy

Fig. 3 shows the overall diagram of the proposed distributed coordination approach to coordinate the building zones with different thermal storage capacities and dynamics in responding to the smart grid. It relies on the multi-agent modeling and the thermal battery modeling of multiple thermal zones and consists of two components: 1) the average consensus-based distributed sensing module and 2) the weighted consensus-based distributed allocation module. In the first step, the average consensus-based distributed sensing module estimates the average thermal SoC of total zones by distributed means,

which is mixed with the estimated thermal storage capacities to derive the weight factors necessary in the weighted consensus-based distributed allocation module. In the second step, the distributed allocation module enables each agent to make local decisions with global coordination by distributed means based on the mixed weight factors. As a result, the DR tasks or the limited heat water are allocated to each zone by fully distributed means and neighbor-to-neighbor communications.

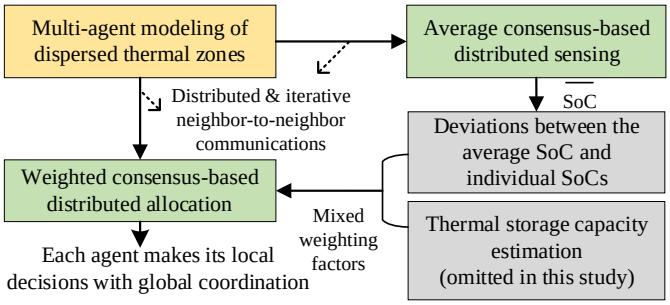

Fig. 3: Overall diagram of the proposed distributed coordination strategy

A. Multi-agent and thermal battery modeling of thermal zones

First, this subsection presents the multi-agent modeling and thermal battery modeling of multiple thermal zones to cope with the proposed distributed coordination strategy.

1) Multi-agent and networked modeling of multiple dispersed thermal zones: Consider multiple air conditioning zones that are geographically dispersed. Each zone is viewed as an agent with a local controller that adjusts the inverter frequency of IACs or valve opening of radiators to respond to external DR requests. We assume a communication network links these zones or agents with specific typologies (e.g., Fig. 4). The operations distributed at different agents are coordinated through neighbor-to-neighbor information exchanges in the communication network. Assuming the adjacent nodes can communicate with each other bidirectionally, the communication network for creating links among zones can be expressed by a graph $G(\vartheta, \zeta)$, where $\vartheta = \{v_1, \ldots, v_r\}$ is a set of nodes, and $\zeta \subseteq \vartheta \times \vartheta$ is a set of edges. A link $(i, j) \in \zeta$ entails information access of node j by node i.

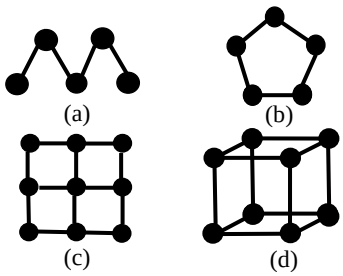

Fig. 4: Communication network typologies of multiple zones (a) linear, (b) ring, (c) rectangle grid, and (d) cube grid

2) Thermal battery modeling of thermal zones: the passive thermal storage of building zones can be modeled and dispatched as a 'thermal battery' model [27], [30]. Consider a thermal zone with a space cooling system, the thermal storage capacity and the thermal 'state of charge (SoC)' of the zone are defined in (1) and (2) by [27], [30], where $C_{a,i}$ is the heat capacity of the air in the i^{th} zone, T_i^{upper} and T_i^{lower} are the indoor temperature range to guarantee the users' thermal comfort, and T_i^t is the real-time zone temperature.

$$E_{cap,i} = C_{a,i}(T_i^{upper} - T_i^{lower}) \tag{1}$$

$$SoC_i = \frac{C_{a,i}(T_i^{upper} - T_i^t)}{C_{a,i}(T_i^{upper} - T_i^{lower})} = \frac{T_i^{upper} - T_i^t}{T_i^{upper} - T_i^{lower}} \tag{2}$$

B. Average consensus-based distributed sensing of the average thermal states of charges (SoC)

Second, a distributed sensing scheme is developed to estimate the average thermal SoC of multiple zones based on the average consensus (AC) algorithm by distributed means and neighbor-to-neighbor communications only.

1) Mathematics of the average consensus algorithm: Average consensus algorithm is a fully distributed information discovery process. The main idea is to share each agent's local thermal SoC information with its neighbors in a distributed and iterative manner through which each agent can estimate the average thermal SoC of a multi-agent network. The information exchange law is defined as (3)

$$x_i[k+1] = x_i[k] + \sum_{j \in N_i} a_{ij}(x_j[k] - x_i[k]) \tag{3}$$

where $i, j \in \{1, \ldots, r\}$ are the indices of r zones, $x_i[k]$ and $x_i[k+1]$ are the network state information discovered by the agent i at the k and k+1 iteration, respectively, a_{ij} is the communication coefficient between the neighbor agents i and j and N_i is the set of neighbor agents connected to agent i. The information exchange for the network can be written in matrix form (4).

$$\mathbf{x}[k+1] = \mathbf{D}\mathbf{x}[k] \tag{4}$$

where $\mathbf{x}[k] = [x_1[k], \ldots, x_n[k], \ldots, x_r[k]]^T$ and $\mathbf{x}[k+1]$ are the state vectors at the k and k+1 iteration, respectively, and $\mathbf{D}$ is a weight matrix (5) with the sparsity pattern specified by the communication graph G.

$$\mathbf{D} = \begin{bmatrix} 1 - \sum\limits_{j \in N_1} a_{1j} & \cdots & a_{1i} & \cdots & a_{1r} \\ \cdots & \cdots & \cdots & \cdots & \cdots \\ a_{i1} & \cdots & 1 - \sum\limits_{j \in N_i} a_{ij} & \cdots & a_{ir} \\ \cdots & \cdots & \cdots & \cdots & \cdots \\ a_{r1} & \cdots & a_{ri} & \cdots & 1 - \sum\limits_{j \in N_r} a_{rj} \end{bmatrix} \tag{5}$$

If the sums of $\mathbf{D}$'s rows and columns are equal to one and the eigenvalues of $\mathbf{D}$ satisfy $\lambda^{\mathbf{D}} \leq 1$, we have (6) based on the *Perron-Frobenius Lemma* [31] with $\mathbf{1}' = \{1, 1, ..., 1\}'$.

$$\mathbf{J} = \lim_{k \to \infty} \mathbf{D}^k = \frac{\mathbf{1} \cdot \mathbf{1}'}{r} \tag{6}$$

This property of the $\mathbf{D}$ matrix implies that the system will reach average consensus (7) as the iteration number k approaches infinity. The average values of global network state

information ($\mathbf{x}[0]$) can be obtained by each agent in a distributed and iterative manner.

$$\lim_{k\to\infty}\mathbf{x}[k]=\lim_{k\to\infty}\mathbf{D}^k\mathbf{x}[0]=\frac{\mathbf{1}\cdot\mathbf{1}^{'}}{r}\mathbf{x}[0] \tag{7}$$

Here, the $\mathbf{D}$ is determined by the *mean metropolis* method [32] with the following law (8) due to the properties of stability, adaptivity, and fast convergence speed.

$$a_{ij}=\begin{cases}2/(g_i+g_j+1) & j\in N_i\\ 1-\sum_{i\in N_i}2/(g_i+g_j+1) & i=j\\ 0 & otherwise\end{cases} \tag{8}$$

where g_i and g_j are the number of agents connected to agents i and j, respectively. According to (7), the average quantities ($\overline{\mathbf{x}}$) can be obtained by each agent in a distributed and iterative manner. Since the iterations cannot go to infinity, a user-defined error tolerance (E_{ac}) is used to reach a consensus. The required number of iterations for convergence (K_{ac}) can be approximately determined by (9) [33]

$$K_{ac}=\min\left\{k\mid\frac{\|\mathbf{x}[k]-\overline{\mathbf{x}}\|}{\|\mathbf{x}[0]-\overline{\mathbf{x}}\|}\le E_{ac},k>0\right\} \tag{9}$$

where E_{ac} is the error tolerance, $\overline{\mathbf{x}}$ is the vector with averaged values and K_{ac} is the minimum number of iterations for convergence under termination criteria.

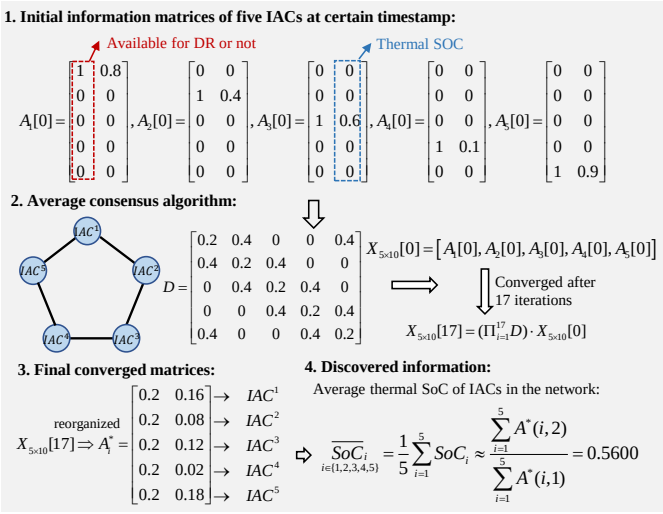

Fig. 5: Illustration of the distributed SoC sensing algorithm for a network of five zones with a ring graph

2) Application of the average consensus algorithm for distributed SoC sensing: Fig. 5 demonstrates the application of the average consensus algorithm for distributed average SoC sensing of five thermal zones. The number of connected thermal zones and their individual SoCs are required to calculate the average SoCs of the network. To obtain this information, each zone agent is initialized with an $A_{5\times2}[0]$ matrix. In matrix $A[0]$, only the rows corresponding to the agents' number can have nonzero elements. $A[0](i,1)$ is equal to either 1 or 0 to represent whether the agent can provide a demand response or is eligible for energy resources, and $A[0](i,2)$ is equal to its thermal SoC.

By applying the average consensus law (7) to each initial matrix, all the information matrices converge to the same final matrix A^*. Each element of A^* is the average summation of the corresponding elements in the five initial matrices. The number of agents is revealed by counting the number of nonzero elements in the first column of A^*. The average SoCs of all zones ($\overline{SoC}$) are discovered by taking the ratios of the second-column summation to the first column by (10).

$$\overline{SoC}=\frac{1}{r}\sum_{i=1}^{r}SoC_i\approx\frac{\sum_{i=1}^{r}A^*(i,2)}{\sum_{i=1}^{r}A^*(i,1)} \tag{10}$$

C. Weighted consensus-based distributed allocation

Next, a weighted consensus (WC) based distributed tasks/resource allocation scheme is developed for demand flexibility coordination.

1) Modeling of the distributed DR tasks/resources allocation problem: Consider a DR task allocation or limited energy resources allocation problem, multiple thermal zones are coordinated to participate in the demand response program or obtain the limited energy sources proportional to their capacities and real-time dynamics. We assume the total amount of resources and tasks are known, and the goal is to allocate the issued DR tasks or limited energy resources (Y^t) to r agents in the network, denoted as $\mathbf{y}^t=[y_1^t,\ldots,y_i^t,\ldots,y_r^t]^{'}$. Consequently, we have the constraint (11). For notation convenience, the timestep superscript is omitted in the following content, i.e., $\mathbf{y}^t\Leftrightarrow\mathbf{y}=[y_1,\ldots,y_i,\ldots,y_r]^{'}$.

$$\sum_{i=1}^{r}y_i^t=Y^t \tag{11}$$

The target of the WC-based distributed tasks/resource allocation scheme is to allocate the DR tasks/resources proportional to the weight factors by distributed means through iterative neighbor-to-neighbor communications, i.e., $\frac{y_i}{\gamma^i}\to\alpha,i=1,\ldots,r$, where γ^i is the corresponding weight factor, y_i is the task/resource allocation variable of i_{th} zone, and α is some constant value.

Let $\mathbf{\Gamma}=[\gamma^1,\ldots,\gamma^r]^{'}$ be the weighting vector of thermal zones, $\mathbf{\Psi}$ be the diagonal matrix $diag[\frac{1}{\gamma^1},\ldots,\frac{1}{\gamma^r}]$, and $\mathbf{1}$ be the column vector of all ones. Together with constraint (11), we can write the target of the WC-based distributed allocation scheme in matrix form: $\mathbf{\Psi y}\to\alpha\mathbf{1}$ subject to $\mathbf{1}^{'}\mathbf{y}=Y$. It follows from $\mathbf{\Gamma}^{'}\mathbf{\Psi}=\mathbf{1}^{'}$ that $\alpha=\frac{Y}{\mathbf{\Gamma}^{'}\mathbf{1}}=\frac{Y}{\gamma^1+\cdots\gamma^r}$. As the iterations go on, the weighted allocation value of the i^{th} agent will converge: $\lim_{k\to\infty}y_i^k\to\alpha\gamma^i$, guaranteeing fair tasks/resource allocation. For the matrix form at the network level, the allocation vector will converge: $\lim_{k\to\infty}\mathbf{y}^k\to\frac{\mathbf{\Gamma}\mathbf{1}^{'}}{\mathbf{\Gamma}^{'}\mathbf{1}}\mathbf{y}^0,\mathbf{1}^{'}\mathbf{y}^0=Y$.

2) Mathematics of the weighted consensus algorithm: The main formulas of the WC algorithm are described below. For each control interval t, the WC algorithm is run for several iterations $k\in\{1,...,K\}$ to achieve convergence. In each iteration step, the allocation variable of i^{th} agent is updated from $y_i[k]$ to $y_i[k+1]$ by the amount $u_i[k]$ (12).

$$y_i[k+1]=y_i[k]+u_i[k] \tag{12}$$

Then, the $u_i[k]$ can be calculated using the link control signal, $\theta_{ij}[k]$, considering the information from neighbor units [34], [35].

$$u_i[k] = -\sum_{(i,j)\in\zeta} \theta_{ij}[k] + \sum_{(j,i)\in\zeta} \theta_{ji}[k] \tag{13}$$

The control signal $\theta_{ij}[k]$, is calculated by (14), which reflects the difference between weighted allocation variables of agents i and j at both sides of the communication link (v_i, v_j) [35].

$$\theta_{ij}[k] = \frac{y_i[k]}{\gamma^i} - \frac{y_j[k]}{\gamma^j} \tag{14}$$

For a better presentation of the above process, (12)-(14) can be written in the following compact matrix form [35]:

$$\begin{gathered} \mathbf{y}[k+1] = \mathbf{y}[k] + \mathbf{u}[k] \\ \Theta[k] = \mathbf{H}_2\mathbf{\Psi}\mathbf{y}[k] - \overline{\mathbf{\Psi}}\mathbf{H}_1\mathbf{y}[k] = \mathbf{H}\mathbf{y}[k] \\ \mathbf{u}[k] = -(\mathbf{H}_2 - \mathbf{H}_1)'\mathbf{H}\mathbf{y}[k] \\ \mathbf{y}[k+1] = \mathbf{M}\mathbf{y}[k], \mathbf{M} = (\mathbf{E} - (\mathbf{H}_2 - \mathbf{H}_1)'\mathbf{H}) \end{gathered} \tag{15}$$

where $\mathbf{E}$ is the identity matrix, $\mathbf{H}_1$ and $\mathbf{H}_2$ are $l_s \times r$ matrices and l_s is the total number of communication links in ζ. If the communication link (v_i, v_j) is the m^{th} link in ζ, then all the elements of m^{th} row in $\mathbf{H}_1$ are zero except the j^{th} element, which is one. All the elements of the m^{th} row in $\mathbf{H}_2$ are zero except the i^{th} element, which is one. $\mathbf{\Psi}$ is $diag[\frac{1}{\gamma^1}, \ldots, \frac{1}{\gamma^r}]$ and $\overline{\mathbf{\Psi}}$ is a $l_s \times l_s$ diagonal matrix whose m^{th} diagonal element is $\frac{1}{\gamma^j}$, if the m^{th} link in the ζ set is (v_i, v_j).

It is proved [34], [35] that the sum of allocation adjustment values ($\mathbf{1}'\mathbf{u}[k]$) always equals zero for all iterations $k \in \{1, \ldots, K\}$. Therefore, the summation of allocation values at each iteration remains unchanged in the WC algorithm (16).

$$\sum_{i=1}^{r} y_i[1] = ... = \sum_{i=1}^{r} y_i[k] = ... \sum_{i=1}^{r} y_i[K] = ... = Y \tag{16}$$

Similar to the average consensus algorithm, the state transition matrix of the weighted consensus algorithm $\mathbf{M}$ is convergent: $\mathbf{B} = \lim_{k\to\infty} \mathbf{M}^k = \frac{\mathbf{\Gamma 1}'}{\mathbf{\Gamma}'\mathbf{1}}$. Since the iterations cannot go to infinity, a user-defined error tolerance (E_{wc}) is used to reach a consensus. The required iterations for convergence can be approximately determined by (17) [33]:

$$K_{wc} = \min\left\{ k \mid \frac{\|\mathbf{y}[k] - \mathbf{y}_{\text{inf}}\|}{\|\mathbf{y}[0] - \mathbf{y}_{\text{inf}}\|} \le E_{wc}, k > 0 \right\} \tag{17}$$

where E_{wc} is the error tolerance, $\mathbf{y}_{inf}$ is the ideal converged vector, and K_{wc} is the minimum number of iterations for convergence under termination criteria.

3) Sufficient condition for converging the weighted consensus algorithm: In our numerical experiments, it is found that the weighted consensus algorithm cannot converge when the weight factors were normalized within the range of [0,1]. While none of the current research discussed the sufficient condition for the convergence of the weighted consensus algorithm. This subsection derives a sufficient condition for selecting weight factors to ensure the convergence of the weighted consensus algorithm - *if the minimum weighting factor of nodes is greater than two times the maximum node degree of communication graphs, the convergence of the weighted consensus algorithm is guaranteed* (18).

$$\min(\mathbf{\Gamma}) \ge 2 \cdot deg \tag{18}$$

where $\mathbf{\Gamma}$ is the weighting vector, deg is the maximum node degree of the communication graph, representing the maximum number of edges connected to a node. The detailed derivation process of (18) is given in the Appendix A.

D. Weighted control by the thermal storage capacity and thermal 'SoC' of zones

Finally, the proposed distributed coordination strategy is adopted in two case studies for DF coordination.

1) Weighted DR participation of IACs by distributed coordination strategy: As shown in equation (19), consider a total power adjustment signal (dP) derived by subtracting the forecasted base load of total IACs (P_L^{base}) from the utility load following signals (P_{LF}) [2], [11], the DR tasks are allocated to each IAC proportional to their weight factors ($[\gamma^1, \gamma^2, \ldots, \gamma^r]$).

$$dP = P_{LF} - P_L^{\text{base}}, \sum_{i=1}^{r} dp_i = dP, \frac{dp_1}{\gamma^1} = \frac{dp_2}{\gamma^2} = \cdots = \frac{dp_r}{\gamma^r} \tag{19}$$

Next, the weight factors are determined by (20) based on the zones' thermal storage capacities ($E_{cap,i}$), the deviation between the average thermal SoC of all zones and the individual real-time SoCs ($s_i = \overline{SoC} - SoC_i$), and the tunable parameters (k_1, k_2). Assume the IACs operate at the cooling mode, and lower temperatures mean higher SoC values by (2). Zones that have higher SoCs than the average SoC of total zones are prioritized for down-regulation reserve ($dP < 0$). Zones that have lower SoCs than the average SoC of total zones are prioritized for up-regulation reserve ($dP > 0$).

$$\gamma^i = \begin{cases} E_{cap,i} \cdot k_1 (1+s_i)^3 \, dP > 0 \\ E_{cap,i} \cdot k_2 (1-s_i)^3 \, dP < 0 \end{cases}, s_i = \overline{SoC} - SoC_i \tag{20}$$

Then, the power adjustment signal of each IAC is translated into inverter frequency adjustment values proportional to the weight factors (21).

$$du_i = \frac{dp_i}{k_3}, \frac{du_1}{\gamma^1} = \frac{du_2}{\gamma^2} = \cdots = \frac{du_r}{\gamma^r} \tag{21}$$

where $E_{cap,i}$ is the thermal storage capacity of i^{th} zone, which can be modeled by the lumped thermal parameter [27] and the details are omitted here. du is the IACs' frequency adjustment value, and k_3 is a tunable parameter.

2) Weighted heat redistribution of primary constant-secondary variable building water heating system by distributed coordination strategy: As shown in Fig. 6, the hot water flow redistribution scheme employs a distributed coordinator to continuously adjust the setpoints of hot water flow rates of individual zones during DR periods. The valves before and after the DR period are controlled through conventional demand feedback controls to maintain the initial indoor temperature setpoints. During the DR period, a designed water flow distributor directly controls the radiators' water flow rates at the real-time updated setpoints by modulating the flow control valves. The given water flow setpoints of individual zones (m_i) are determined by (22), where M is the constant primary-loop water flow rate, s_i is the deviation between the estimated average thermal SoC ($\overline{SoC}$) of the network with individual zones' SoCs (SoC_i), $E_{cap,i}$ is the estimated thermal

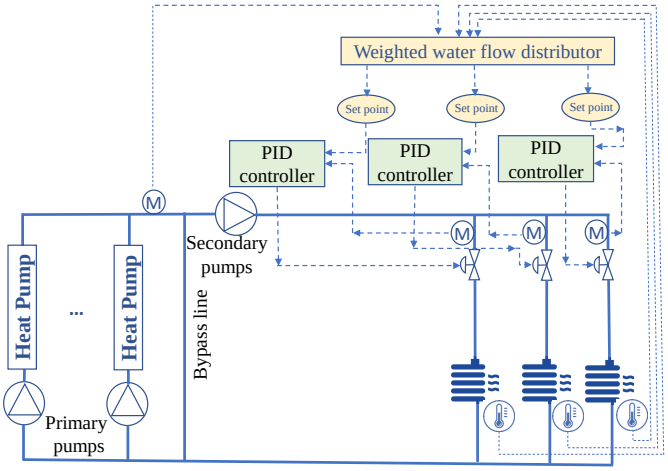

Fig. 6: Application of distributed coordination strategy to the primary constant-secondary variable building water heating system in urgent DR requests

storage capacity, γ^i is the weight factor related to the thermal storage capacities and real-time dynamics and k_4 is a tunable parameter.

$$\sum_{i=1}^{r} m_i = M, \frac{m_1}{\gamma^1} = \frac{m_2}{\gamma^2} = \cdots = \frac{m_r}{\gamma^r}$$
$$\gamma^i = E_{cap,i} \cdot k_4 (1 - s_i)^2, s_i = \overline{SoC} - SoC_i \quad (22)$$

IV. Simulation Test and Verification

In this section, we verified through numerical examples the performance of distributed sensing and distributed task/resource allocation schemes, the sufficient condition for converging the weighted consensus algorithm, and the scalability to large network sizes of different communication graphs. The communication graphs are ring unless otherwise stated.

A. Performance of the distributed sensing scheme for estimating the average thermal SoCs

Fig. 7a shows the simulated indoor temperatures of five zones and their average. Fig. 7b shows the actual (blue) and estimated (red) thermal SoC profiles of five zones by the distributed sensing scheme. It is observed in Fig. 7b that the estimated average SoC profile is almost the same as the actual average SoC profile, which verified the performance of average consensus algorithm for distributed sensing of average SoC for zones in the network.

B. Performance of the distributed tasks/resources allocation scheme based on the weighted consensus algorithm

Fig. 8 shows the verification results of the weighted consensus algorithm for distributed DR tasks allocation of five zones. Let's assume the requested DR amount by the grid operator at a certain timestep is 50 kW, and there are five zones to respond to the DR signals. The weighting factors of five zones are set as $\mathbf{\Gamma} = [10, 20, 30, 40, 50]$, respectively, and the distributed allocation scheme is utilized for DR task allocation. The initial allocation vector is assigned as random values summed to 50kW. As the iterations of the weighted consensus algorithm go on, the allocation vector will approach the consensus

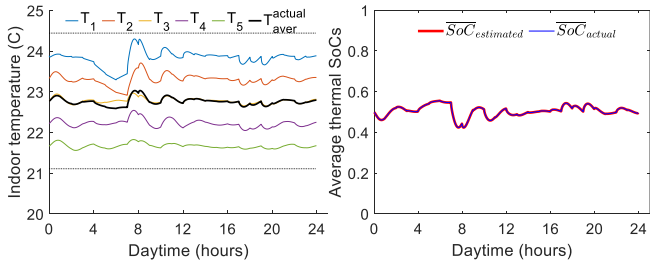

(a) (b)

Fig. 7: (a) indoor temperatures of five simulated zones and their average profile and (b) a comparison between actual and estimated average thermal SoCs of five zones

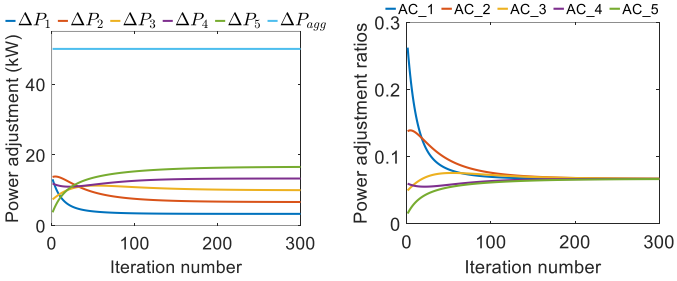

(a) (b)

Fig. 8: Verification of distributed tasks/resources allocation scheme: (a) trajectories of power adjustments; (b) trajectories of power adjustment ratios;

allocation vector with values proportional to their weight factors. Fig. 8a shows the actual power adjustments made by each zone. It is seen that the DR allocations always sum to the initial total value (i.e., 50 kW), and the agents quickly achieve consensus within one hundred iterations. The power adjustments are also proportional to their weighting factors. Fig. 8b shows that the five zones approach the same power adjustment ratios ($\frac{dp_i}{\gamma^i}$) after iterative communications.

TABLE II: weight factors selection for converging the weighted consensus algorithm

communication graphs	path	ring	rectangular grid	cube grid
deg	2	2	4	6
$\min(\mathbf{\Gamma})$	4	4	8	12

C. Verification of the sufficient condition to converge the weighted consensus algorithm

We found that if the weight factors are normalized within [0,1] or taken as [1,2,3,4,5] for the five zones in the simulation of IV-B, the WC algorithm cannot converge. Thus, we derive the sufficient condition in (18) for converging the WC algorithm. Table II lists the maximum node degree (deg) of four types of communication graphs in Fig. 4 and the corresponding minimum weight factors to guarantee the convergence of WC. For example, the maximum node degree of the ring graph is two. If we scale the weighting factors by ten to satisfy: $\min(\mathbf{\Gamma}) \geq 4$ (i.e., [10,20,30,40,50]), the convergence of the WC algorithm is guaranteed in the simulation of IV-B.

D. Scalability to large network sizes of different communication typologies

This section presents the required iterations of distributed sensing and allocation schemes for different communication graphs in Fig. 4 with increasing network sizes. The iterations numbers are obtained based on (9) and (17) for the same error tolerance ($E_{wc} = E_{ac} = 1E-5$) by randomly assigning the initial states of agents with a summation of 50 and the weight factors satisfying the condition (18).

Table III shows the required iterations of the distributed sensing scheme under the termination criteria. It is observed that the required iterations of linear and ring graphs significantly increase with network sizes and become unacceptable when the number of agents exceeds 64. While the required iterations of the rectangular and cube graphs increase at a much smaller rate with the network sizes, and they are acceptable even for 1000 zones. Table IV shows a similar pattern for the distributed DR tasks/resources allocation scheme. The convergence speed of the distributed sensing scheme is slightly better than the distributed allocation scheme when comparing Tables III and IV. We concluded that the required iterations for linear and ring graphs increase dramatically with the network sizes, and they only apply to small networks with less than one hundred zones due to the graphs' poor connectivity. The graphs with rectangle and cube grid typologies have smaller iteration numbers, increasing slowly with the network sizes. Due to the graphs ' good connectivity, they can apply to larger networks with nearly 1000 zones.

For the average consensus algorithm, one agent needs to calculate $3N_i$ floating-point operations (FLOPs) for one iteration, i.e., equation (3), where N_i is the number of neighbor agents connected to the agent. For the weighted consensus algorithm, one agent needs to calculate $6N_i$ FLOPs for one iteration, i.e., equations (12)-(14). The total FLOPs of $1E+3$ iterations of one agent are estimated as $(18 \sim 54) \times 1E+3$ for the communication graphs in Fig. 4, which are far less than the floating-point operations per second (FLOPS) of typical embedded micro-controllers. For example, the TMS320F28335 (a real-time micro-controller of TEXAS INSTRUMENTS) operates at speeds up to 150 megahertz (MHz) and can perform 300 million FLOPS ($3 \times 1E8$ FLOPs per second) [36].

TABLE III: Scalability of distributed SoC sensing scheme for graphs with increasing network sizes

Network sizes		8	64	125	1000
Required number of iterations for one consensus	Linear	**148**	9669	34865	1.89E+06
	Ring	**36**	2319	7267	4.75E+05
	Rectangle Grid	**45**	**266**	2282	5043
	Cube Grid	**24**	**71**	**129**	**492**

E. Convergence speed comparison between the average consensus algorithm and the Alternating Direction Method of Multipliers (ADMM) method

For comparing the convergence speeds between the average consensus method and the ADMM method, the ADMM method is also used to solve the same distributed averaging problem and cast into a similar matrix form to the average consensus algorithm so that the convergence properties can be easily analyzed and compared, as summarized in Table V. The derivation details are given in Appendix B.

TABLE IV: Scalability of distributed DR tasks/resources allocation scheme for graphs with increasing network sizes

Network sizes		8	64	125	1000
Required number of iterations for one consensus	Linear	**554**	26525	79236	6E+06
	Ring	**117**	8023	28284	3E+06
	Rectangle Grid	**133**	**483**	3042	9746
	Cube Grid	**36**	**124**	**180**	**672**

TABLE V: The application of ADMM and average consensus methods for distributed sensing and their matrix forms

	Average consensus	ADMM
State transition matrix	$\mathbf{x}[k+1] = \mathbf{D} \cdot \mathbf{x}[k]$ $\mathbf{D}$ is given in (5)	$\begin{cases} \begin{bmatrix} \mathbf{x}[k+1] \\ \mathbf{x}[k] \end{bmatrix} = \underbrace{\begin{bmatrix} \mathbf{M} & -\mathbf{H} \\ \mathbf{I}_r & \mathbf{0}_r \end{bmatrix}}_{\mathbf{F}} \begin{bmatrix} \mathbf{x}[k] \\ \mathbf{x}[k-1] \end{bmatrix} \\ \mathbf{x}[0] = 0, \mathbf{x}[1] = (\mathbf{I}_r - \mathbf{P})\,\boldsymbol{\theta} \end{cases}$ $k \geq 1, \mathbf{M} = \mathbf{I}_r + \mathbf{P} + 2\mathbf{U}, \mathbf{H} = \mathbf{P} + \mathbf{U}$ $\mathbf{P} := \operatorname{diag}(\mathbf{W}\mathbf{1}_r) \operatorname{diag}(\mathbf{A} + \mathbf{W}\mathbf{1}_r)^{-1}$ $\mathbf{U} := \operatorname{diag}(\mathbf{A} + \mathbf{W}\mathbf{1}_r)^{-1} W \cdot$ $\operatorname{diag}\left(\mathbf{1}_r{}^T \mathbf{W}\right)^{-1} \mathbf{W}^T - \mathbf{P}$ $\mathbf{A} = [a_1, a_2, \ldots, a_r]^T, \mathbf{W} = \mu \mathbf{D}, \mu > 0$
Convergence rate	$\rho_{\mathbf{D}}$	$\rho_{\mathbf{F}}$

The convergence rates of the average consensus and ADMM algorithms are determined by the essential spectral radius of the graphs' state transition matrix ($\rho_{\mathbf{D}}$,$\rho_{\mathbf{F}}$), which corresponds to the absolute value of the matrix's eigenvalue with the second largest magnitude ($\rho = \max\{|\lambda_2, \lambda_N|\}, \lambda_1 = 1 > \lambda_2 \geq \cdots \geq \lambda_N > -1$). Graphs with a large number of agents and sparse communication edges have ρ close to one, while for dense graphs have ρ close to zero. Higher values of essential spectral radius mean higher iterations for convergence. By plotting the convergence rates of ADMMs and the average consensus algorithms as a function of the convergence rates of the average consensus algorithm (i.e., Fig. 9 and 10), it is convenient to compare the theoretical convergence speed between ADMMs and average consensus. For the simulations in Fig. 9, the ring graphs with increasing agents from three to 100 are considered for the distributed averaging problem. The ring graph with three agents is complete and has $\rho = 0$, while the ρ of ring graphs quickly increases close to one with the increasing number of agents. For the simulations in Fig. 10, the cube graphs are comprised of 1000 agents, which are evenly distributed in a cube environment with unit length edge, and the distance threshold ($thre$) for two agents to be connected varies between $\frac{1}{9}$ and $\sqrt{3}$. Note that the cube graph is the same as Fig. 4d when the distance threshold is $\frac{1}{9}$, and the essential spectral radius $\rho_{\mathbf{D}}$ reduces with the increased distance thresholds and equals zero when the distance threshold exceeds $\sqrt{3}$.

In Fig. 9 and 10, the colored curves above the black dotted line mean the ADMM-based methods have slower convergence rates than the average consensus-based methods and vice versa. It is observed that the ADMM-based method's perfor-

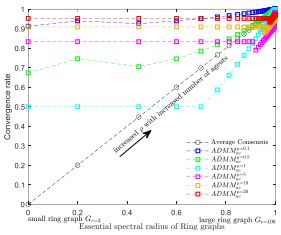

Fig. 9: Theoretical convergence rate of the ADMM solution as a function of the convergence rate of the average consensus solution for ring graphs with increasing network size from the bottom left (r=3) to the top right (r=100)

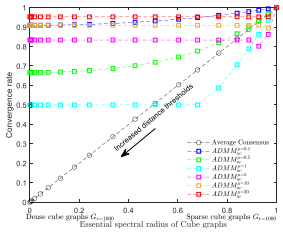

Fig. 10: Theoretical convergence rate of the ADMM solution as a function of the convergence rate of the average consensus solution for cube grid graphs with increasing distance thresholds from the bottom left ($thre$=$\frac{1}{9}$) to the top right ($thre$=$\sqrt{3}$)

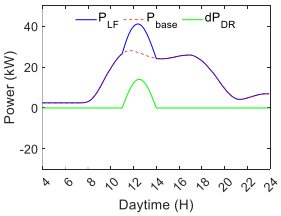

Fig. 11: Demand response signals for case study I

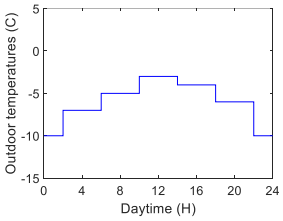

Fig. 12: Outdoor temperature profiles for case study II

mance is sensitive to the algorithm parameter selection (μ). A poor choice of the ADMM algorithm parameter could result in worse performance than the average consensus algorithm (i.e., the green curves in Fig. 9 and 10 with μ=0.5). For ring graphs with small edge density, ADMM is a better choice for networks with a large number of agents when the ADMM algorithm parameter is selected correctly (i.e., the sky-blue curve on the top right of Fig. 9 with μ=1). When the network size is large, i.e., 1000 zones, and the ADMM algorithm parameter is appropriately selected, ADMM is an excellent algorithm to apply in graphs with small edge densities (i.e., the sky-blue curve on the top right of Fig. 10 with μ=1). However, it becomes less competitive than the average consensus algorithm when the edge densities are increased (i.e., the sky-blue curve on the bottom left of Fig. 10).

V. Results of Application Case Studies

This section illustrates the results of applying the distributed coordination strategy to two application case studies.

A. Case study I: distributed coordination of multiple IACs

For case study I, five IAC units with thermal mass ratios of 1:2:3:4:5 are modeled in MATLAB by ETP models with heterogeneous parameters and shifted and scaled solar and internal heat gains. They are coordinated to respond to the load following (LF) signals in Fig. 11.

Fig. 13 shows the consensus control performance by only weighting the thermal storage capacities. Fig. 13a and Fig. 13b show the inverter frequencies and the inverter frequency adjustments of five IACs, and Fig. 13c and Fig. 13d show the indoor temperatures and associated thermal SoC profiles of five zones. It is observed that the inverter frequencies increase with the same ratios as the thermal storage capacities during the DR period from 11:00 am to 14:00 am. The corresponding indoor temperatures quickly decrease at different rates. The indoor temperatures of zone-4 and zone-5 drift outside the lower temperature limits, which may sacrifice the users' comfort and induce the drop out of the DR program for zone-4 and zone-5. Zone-1 and zone-2 still have enough flexible resources when the temperatures of zone-4 and zone-5 decrease below the lower temperature limit and deplete their thermal flexibility.

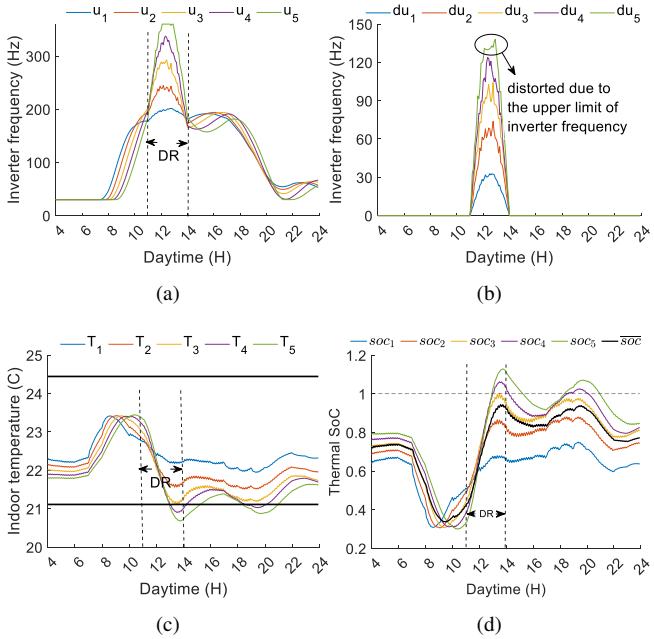

Fig. 13: Consensus control weighted by only thermal storage capacities (a) inverter frequency of five IACs, (b) inverter frequency adjustments proportional to thermal storage capacities, i.e., $du_1 : du_2 : du_3 : du_4 : du_5 = E_{cap,1} : E_{cap,2} : E_{cap,3} : E_{cap,4} : E_{cap,5} = 1 : 2 : 3 : 4 : 5$), (c) indoor temperatures of five zones, (d) thermal SoCs.

Fig. 14 shows the consensus control performance by weighting the thermal storage capacities and the real-time thermal SoCs. Fig. 14a and Fig. 14b show the inverter frequencies and the inverter frequency adjustments of five IACs, and Fig. 14c and Fig. 14d show the indoor temperatures and associated thermal SoC profiles of five zones. It is observed that the increases in inverter frequencies vary a lot with the real-time thermal SoCs instead of being proportional to their thermal storage capacities only. Thus, the indoor temperatures of the five zones are decreasing in a more concentrated manner. The indoor temperatures of zone-4 and zone-5 still fall within the users' thermal comfort zone when the same DR requests are fulfilled. The thermal flexibility of zone-1 and zone-2 is prioritized for usage as the temperatures of the other three zones approach the lower temperature limits.

B. Case study II: weighted water flow redistribution

For case study II, a commercial primary constant-secondary variable building water heating system in Fig. 6 is simulated in MATLAB/Simulink to solve the redistribution problem of limited hot water during urgent DR periods. The assumed

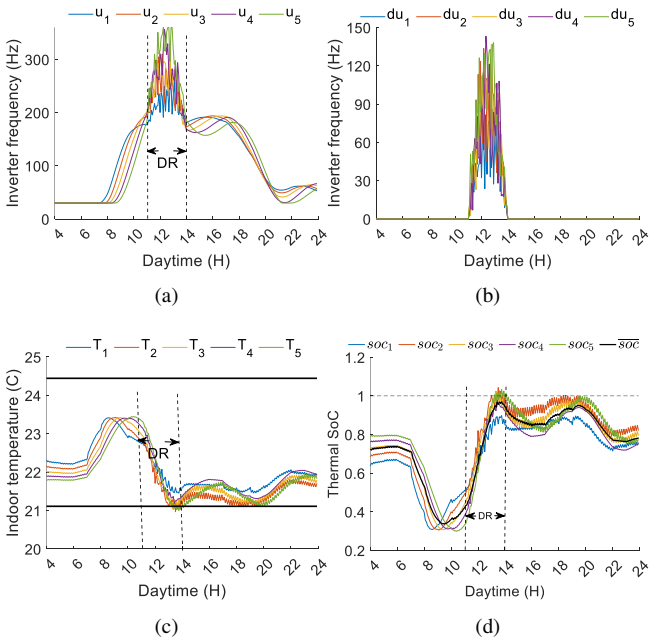

Fig. 14: Consensus control weighted by both thermal storage capacities and thermal SoCs (a) inverter frequency of five IACs, (b) inverter frequency adjustments proportional to thermal storage capacities and thermal SoCs, i.e., $\frac{du_1}{\gamma^1} = \frac{du_2}{\gamma^2} = \frac{du_3}{\gamma^3} = \frac{du_4}{\gamma^4} = \frac{du_5}{\gamma^5}, \gamma^i = F\left(E_{cap,i}, SoC_i, \overline{SoC}\right)$, (c) indoor temperatures of five zones, (d) thermal SoCs.

weather data is a typical winter day in a cold area in Fig. 12. We assume half of the central heat pumps are shut down during the DR periods between 11:00 and 12:00am. The proposed distributed coordination strategy is used to redistribute the hot water flow during urgent DR events and achieve uniform temperature variations.

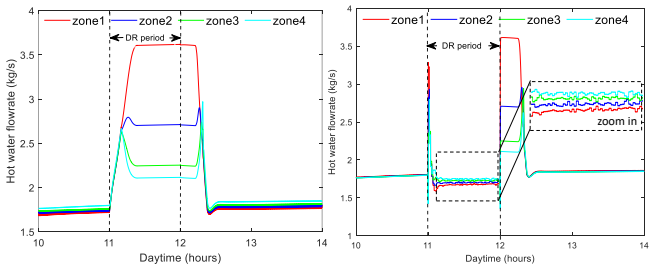

Fig. 15: Water flow rate profiles of four zones for (a) conventional control strategy and (b) proposed coordination strategy

Fig. 15 compares the hot water flow rates distributed to individual zones using conventional and coordinated control strategies. Under the conventional control strategy, all thermal zones compete for the limited hot water supply when half of the heat pumps are shut down for fast demand response. Each radiator opens the flow control valve to the maximum, dramatically increasing hot water flow rates. In contrast, the proposed coordination strategy redistributes the limited hot water resources based on the four zones' thermal storage capacities and real-time thermal SoCs. There are no water flow surges during the DR period, and the limited hot water resources are allocated to four zones proportional to their weight factors.

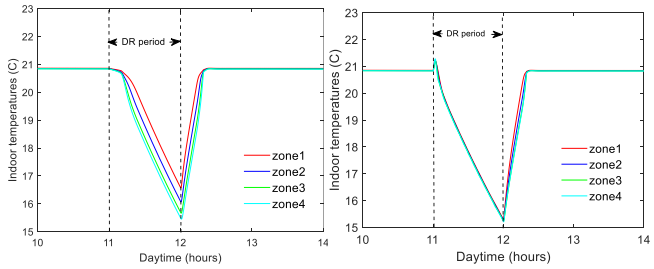

Fig. 16: Indoor air temperature profiles of zones in DR periods using (a) conventional control strategy and (b) proposed distributed coordination strategy

Fig. 16 shows the indoor temperature profiles of four zones using conventional and proposed distributed coordination control strategies. In Fig. 16a, the indoor temperature profiles of the four zones are different during the DR period due to their different pressures and water flow rates in the water heating system. While the temperatures of the four zones using the proposed distributed coordination strategy are almost the same during the DR period in Fig. 16b.

Fig. 17 shows the water flows in the bypass pipe using the conventional and proposed control strategies. The distributed coordination strategy could eliminate the disordered flow and keep the water flow rate in the bypass pipe at about zero during the DR period. Fig. 18 compares the power consumption of secondary water pumps using two control strategies. It is seen the power is further reduced by about $2kW$ (17.9%) using the proposed control strategy, due to the significantly reduced hot water flow rates.

VI. Conclusion

This study develops a novel fully distributed rule-based coordination strategy to coordinate thermal zones with different thermal 'storage capacities' and 'state of charges (SoCs)' in responding to the smart grid for efficient and effective utilization of their limited energy flexibility. It relies on the multi-agent and thermal battery modeling of multiple thermal zones and coordinates the demand flexibility resources

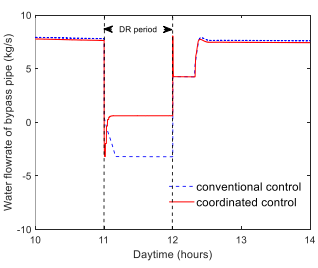

Fig. 17: Water flow rates in bypass pipes using conventional and proposed control strategies

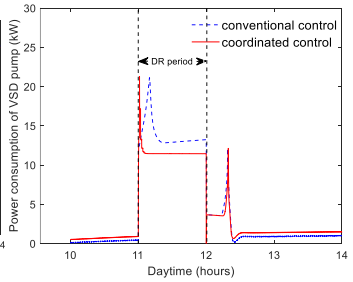

Fig. 18: Power consumption of secondary water pumps using conventional and proposed control strategies

by fully distributed means through a sparse communication network with affordable communication costs, plug-and-play, and privacy protection features. We also derive the sufficient condition for the first time to guarantee the convergence of the weighted consensus algorithm and compare the convergence rates of the average consensus-based and ADMM-based distributed sensing schemes. Numerical experiments validate the effectiveness of the sufficient condition for converging the weighted consensus algorithm and the scalability of the proposed distributed coordination approach when the communication typologies are properly selected and the number of connected agents is reasonable. It is also indicated the consensus-based and ADMM-based distributed control methods may have their computational competitiveness under different situations. Finally, the distributed coordination strategy is adopted in two application case studies in DR events. Simulation results illustrated that the proposed distributed coordination strategy could avoid the early depletion issue of thermal demand flexibility and non-uniform thermal comfort sacrifices in uncoordinated control.

APPENDIX

A. Derivation of the sufficient condition for converging the weighted consensus algorithm

According to (15), the update of the allocation vector for the whole network can be expressed as (23), where $\mathbf{M} = \mathbf{E} - (\mathbf{H}_2 - \mathbf{H}_1)'\mathbf{H}$, $\mathbf{E}$ is the identity matrix and $(\mathbf{H}_2 - \mathbf{H}_1)'$ means the transpose of $\mathbf{H}_2 - \mathbf{H}_1$.

$$\mathbf{y}[k+1] = \mathbf{M}\mathbf{y}[k] \tag{23}$$

Given that $\mathbf{H} = \mathbf{H}_2\mathbf{\Psi} - \overline{\mathbf{\Psi}}\mathbf{H}_1$, $\overline{\mathbf{\Psi}}\mathbf{H}_1\mathbf{\Psi}^{-1}$=$\mathbf{H}_1$, we have (24), with $\mathbf{A} = (\mathbf{H}_2 - \mathbf{H}_1)'(\mathbf{H}_2 - \mathbf{H}_1)$.

$$\mathbf{M} = \mathbf{E} - \mathbf{A}\mathbf{\Psi} \tag{24}$$

If the weighted consensus algorithm converges, the state transition matrix $\mathbf{M}$ must be a convergent matrix satisfying the following condition

$$\lim_{k\to\infty} \mathbf{M}^k = \frac{\mathbf{\Gamma 1}'}{\mathbf{\Gamma}'\mathbf{1}} = \mathbf{B} \Leftrightarrow \lim_{k\to\infty} \mathbf{M}^k - \mathbf{B} = \mathbf{0} \tag{25}$$

The necessary and sufficient condition for the $\mathbf{M}-\mathbf{B}$ matrix that converges to the zero matrix is: $|\lambda_{\max}| = \rho(\mathbf{M}-\mathbf{B}) < 1$, where $|\lambda_{\max}|$ is the eigenvalue of $\mathbf{M}-\mathbf{B}$ with the largest magnitude, and ρ is the spectral radius of $\mathbf{M}-\mathbf{B}$. The proof is omitted here for space concerns.

Since $\mathbf{B} = \frac{\mathbf{\Gamma 1}'}{\mathbf{\Gamma}'\mathbf{1}}$ is element-wise positive, $\mathbf{M}-\mathbf{B}$ is element-wise bounded below by the matrix $\mathbf{M}$, and $(\mathbf{M}-\mathbf{B})^k$ is element-wise bounded below by $\mathbf{M}^k$ for every positive integer k. By using *Gelfand's formula* ($\rho(\mathbf{M}) = \lim_{k\to\infty} \left\|\mathbf{M}^k\right\|^{\frac{1}{k}}$), it follows that $\rho(\mathbf{M}-\mathbf{B}) < \rho(\mathbf{M})$. If we select weighting factors satisfying the condition: $\rho(\mathbf{M}) = \rho(\mathbf{E}-\mathbf{A}\mathbf{\Psi}) \le 1$, the $\mathbf{M}-\mathbf{B}$ matrix is guaranteed to converge to the zero matrix because $\rho(\mathbf{M}-\mathbf{B}) < 1$. According to (26), if the weighting factors are selected to satisfy $0 \le \lambda(\mathbf{A}\mathbf{\Psi}) \le 2$, the convergence of the weighted consensus algorithm is guaranteed, where $\lambda(\mathbf{A}\mathbf{\Psi})$ denotes the eigenvalues of $\mathbf{A}\mathbf{\Psi}$.

$$\begin{gathered} \rho(\mathbf{M}) = \rho(\mathbf{E} - \mathbf{A}\mathbf{\Psi}) \le 1 \\ \Updownarrow \\ -1 \le \lambda(\mathbf{E} - \mathbf{A}\mathbf{\Psi}) \le 1 \\ \Downarrow \lambda(\mathbf{E}) = 1 \\ 0 \le \lambda(\mathbf{A}\mathbf{\Psi}) \le 2 \end{gathered} \tag{26}$$

Next, we derive the sufficient condition for selecting weight factors to satisfy: $0 \le \lambda(\mathbf{A}\mathbf{\Psi}) \le 2$. First, it is easy to prove $\mathbf{A}$ is a positive definite matrix. Thus, $\mathbf{A}$ has a positive definite symmetric square root $\mathbf{A}^{1/2}$. Given that $\mathbf{\Psi}$ is a diagonal matrix with positive entries, $\mathbf{A}^{\frac{1}{2}}\mathbf{\Psi}\mathbf{A}^{\frac{1}{2}}$ is symmetric and positive definite. Then, it can be proved that $\mathbf{A}\mathbf{\Psi} = \mathbf{A}^{\frac{1}{2}}(\mathbf{A}^{\frac{1}{2}}\mathbf{\Psi})$ and $\mathbf{A}^{\frac{1}{2}}\mathbf{\Psi}\mathbf{A}^{\frac{1}{2}}$ have the same eigenvalues by applying ***Lemma 1*** below. Since $\mathbf{A}^{\frac{1}{2}}\mathbf{\Psi}\mathbf{A}^{\frac{1}{2}}$ is a positive definite matrix, $\mathbf{A}\mathbf{\Psi}$ and $\mathbf{A}^{\frac{1}{2}}\mathbf{\Psi}\mathbf{A}^{\frac{1}{2}}$ always has the nonnegative eigenvalues only if the weighting factors are positive.

$$\lambda(\mathbf{A}\mathbf{\Psi}) \ge 0 \tag{27}$$

Second, let v be an eigenvector of the eigenvalue μ of $\mathbf{A}$ matrix, and v_k is the element of v with the largest absolute value ($|v_k| \ge |v_i|, i \in \{1, ..., r\}, i \ne k$). Then, the upper bound of the spectral radius of $\mathbf{A}$ can be determined as $\max(\sum_j |\mathbf{A}_{ij}|)$ by (28).

$$\begin{aligned} &\mathbf{A}v = \mu v \Rightarrow \sum_j \mathbf{A}_{kj} v_j = \mu v_k \\ &|\mu v_k| = |\mu|\,|v_k| = \left|\sum_j \mathbf{A}_{kj} v_j\right| \le \sum_j |\mathbf{A}_{kj}|\,|v_k| \le (\sum_j |\mathbf{A}_{kj}|)\,|v_k| \\ &|\mu| \le \sum_j |\mathbf{A}_{kj}| \Rightarrow \mu \le \sum_j |\mathbf{A}_{kj}| \end{aligned} \tag{28}$$

It is easy to derive from (28) that the spectral radius of $\mathbf{A}$ must satisfy (29)

$$\rho(\mathbf{A}) \le \max(\sum_j |\mathbf{A}_{kj}|) \tag{29}$$

It is also noted that the $\max(\sum_j |\mathbf{A}_{kj}|)$ in (29) always equals $deg \times 4$, where deg is the maximum node degree of communication graphs. If we scale the weighting factors to satisfy (18), we could derive $\lambda(\mathbf{A}\mathbf{\Psi}) \le 2$ in (30).

$$\begin{aligned} &\rho(\mathbf{\Psi}) = \lambda_{\max}^{\mathbf{\Psi}} = \frac{1}{\min(\gamma)} \le \frac{1}{2 \cdot deg} \\ &\rho(\mathbf{A}) \le \max(\sum_j |\mathbf{A}_{ij}|) = 4 \cdot deg \\ &\rho(\mathbf{A}) \cdot \rho(\mathbf{\Psi}) \le 2 \Rightarrow \lambda(\mathbf{A}\mathbf{\Psi}) \le \rho(\mathbf{A}\mathbf{\Psi}) \le \rho(\mathbf{A}) \cdot \rho(\mathbf{\Psi}) \le 2 \end{aligned} \tag{30}$$

Equations (26), (27), and (30) conclude the proof of the sufficient condition in (18).

Lemma 1: If S and T are $n \times n$ matrices, ST and TS have the same nonzero eigenvalues.

Proof: If u is an eigenvector of ST for the eigenvalue w: $STu = wu$, then $TS(Tu) = T(STu) = T(wu) = w(Tu)$. Thus, ST and TS have the same eigenvalues.

B. The application of ADMM for distributed averaging and associated matrix form

First, the distributed averaging problem is equivalent to the following constrained convex optimization problem that can be decomposed and solved by the ADMM method

$$\begin{aligned} &\arg\min_{\{x\}} \sum_{i=1}^{r} f_i(x) \\ &\text{subject to } f_i(x) = \frac{1}{2} a_i \left(x-\theta_i\right)^2, \forall i \in \{1,\ldots,N\} \\ &x \in \Omega_1 \cap \Omega_2 \cap \cdots \cap \Omega_r \end{aligned} \tag{31}$$

where the global cost function is the sum of the cost function of each agent ($f_i(x)$), and the aim of the agents is to collaborate to find the minimizer $x^* \in R$ of the global cost function in a distributed way, communicating with their respective neighbors defined by graph G. The above optimization problem has a closed-form solution:$x^* = \frac{\sum_{i=1}^{r} a_i \theta_i}{\sum_{i=1}^{r} a_i}$.

When the coefficients of the agents' cost functions are the same ($a_i = \overline{a}$), the optimizer of the optimization problem reduces to $x^* = \frac{1}{2}\sum_{i=1}^{r} \theta_i$. This corresponds to distributively finding the average of r numbers θ_i, the same to the average consensus-based distributed sensing module. To solve the above problem using ADMM, an auxiliary vector $\mathbf{z} \in R^r$ is introduced, and the problem is recast in the following form

$$\begin{aligned} &\mathbf{x}^* = \arg\min_{\mathbf{x}} \sum_{i=1}^{r} f_i\left(x_i\right) \\ &\text{subject to } f_i\left(x_i\right) = \frac{1}{2} a_i \left(x_i-\theta_i\right)^2 \\ &x_i = z_j, \forall i, \text{ and } j \in N_i \end{aligned} \tag{32}$$

ADMM exploits the augmented Lagrangian with Lagrangian multipliers $\lambda_{ij} \in R$ and penalty parameters $w_{ij} > 0, i, j = 1,\ldots,r, (i,j) \in \zeta$

$$L(\mathbf{x},\mathbf{z},\mathbf{\Lambda}) = \sum_{i=1}^{r} \frac{1}{2} a_i \left(x_i-\theta_i\right)^2 + \sum_{i=1}^{r} \sum_{j \in N_i} \lambda_{ij}\left(x_i - z_j\right) + \frac{1}{2} \sum_{i=1}^{r} \sum_{j \in N_i} w_{ij}\left(x_i - z_j\right)^2 \tag{33}$$

The standard updates of ADMM are obtained from the Lagrangian imposing first-order optimality condition on the x_i's and z_i's in (33) and using an ascent step for variables λ_{ij}'s

$$x_i[k+1] = \left(a_i + \sum_{j \in N_i} w_{ij}\right)^{-1} \left(a_i\theta_i + \sum_{j \in N_i} \left(w_{ij} z_j[k] - \lambda_{ij}[k]\right)\right) \tag{34}$$

$$z_j[k+1] = \frac{\sum_{i \in N_j} w_{ij} x_i[k+1] + \sum_{i \in N_j} \lambda_{ij}[k]}{\sum_{i \in N_j} w_{ij}} \tag{35}$$

$$\lambda_{ij}[k+1] = \lambda_{ij}[k] + w_{ij}\left(x_i[k+1] - z_j[k+1]\right) \tag{36}$$

Second, the above application of ADMM to the optimization model is cast into a matrix form in (36) where analytical properties of matrices can also be assessed [37]. Like matrix $\mathbf{D}$ of the average consensus algorithm, matrix $\mathbf{F}$ determines the convergence rate of ADMM-based distributed averaging through its second-largest eigenvalue in absolute value. In this paper, we select matrix W as $\mathbf{W} = \mu\mathbf{D}$, with $\mu > 0$ as a tunable algorithm parameter and $\mathbf{D}$ as a symmetric stochastic matrix consistent with the communication graph G of the average consensus algorithm. This choice for matrix $\mathbf{W}$ allows a comparison with the average consensus algorithm built using matrix $\mathbf{D}$. It is seen the theoretical convergence rate of ADMM-based distributed averaging is related to the network topology ($\mathbf{D}$), the properties of local objective functions (a_i), and the algorithm parameter (μ).

$$\begin{aligned} &\begin{cases} \begin{bmatrix} \mathbf{x}[k+1] \\ \mathbf{x}[k] \end{bmatrix} = \underbrace{\begin{bmatrix} \mathbf{M} & -\mathbf{H} \\ \mathbf{I}_r & \mathbf{0}_r \end{bmatrix}}_{\mathbf{F}} \begin{bmatrix} \mathbf{x}(k) \\ \mathbf{x}(k-1) \end{bmatrix}, k \geq 1 \\ \mathbf{x}[0] = 0, \mathbf{x}[1] = \left(\mathbf{I}_r - \mathbf{P}\right)\boldsymbol{\theta} \end{cases} \\ &\mathbf{M} = \mathbf{I}_r + \mathbf{P} + 2\mathbf{U}, \mathbf{H} = \mathbf{P} + \mathbf{U} \\ &\mathbf{P} := \operatorname{diag}\left(\mathbf{W}\mathbf{1}_r\right) \operatorname{diag}\left(\mathbf{A} + \mathbf{W}\mathbf{1}_r\right)^{-1} \\ &\mathbf{U} := \operatorname{diag}\left(\mathbf{A} + \mathbf{W}\mathbf{1}_r\right)^{-1} W \operatorname{diag}\left(\mathbf{1}_r{}^T \mathbf{W}\right)^{-1} \mathbf{W}^T - \mathbf{P} \\ &\mathbf{A} = [a_1, a_2, \ldots, a_r]^T, \mathbf{W} = \mu\mathbf{D}, \mu > 0 \end{aligned} \tag{37}$$

ACKNOWLEDGMENTS

The research is financially supported by a collaborative research fund (C5018-20G) of the Research Grant Council (RGC) of the Hong Kong SAR and a project of the strategic importance of The Hong Kong Polytechnic University.

REFERENCE

[1] R. Jackson, E. Zhou, and J. Reyna, "Building and grid system benefits of demand flexibility and energy efficiency," *Joule*, vol. 5, no. 8, pp. 1927–1930, 2021.

[2] Z. Zheng, S. Wang, W. Li, and X. Luo, "A consensus-based distributed temperature priority control of air conditioner clusters for voltage regulation in distribution networks," *IEEE Transactions on Smart Grid*, 2022.

[3] Y. Zhang, K. Shan, X. Li, H. Li, and S. Wang, "Research and technologies for next-generation high-temperature data centers–state-of-the-arts and future perspectives," *Renewable and Sustainable Energy Reviews*, vol. 171, p. 112 991, 2023.

[4] H. Tang, S. Wang, and H. Li, "Flexibility categorization, sources, capabilities and technologies for energy-flexible and grid-responsive buildings: State-of-the-art and future perspective," *Energy*, vol. 219, p. 119 598, 2021.

[5] L. Cirocco, P. Pudney, S. Riahi, *et al.*, "Thermal energy storage for industrial thermal loads and electricity demand side management," *Energy Conversion and Management*, vol. 270, p. 116 190, 2022.

[6] R. Tang, S. Wang, D.-C. Gao, and K. Shan, "A power limiting control strategy based on adaptive utility function for fast demand response of buildings in smart grids," *Science and Technology for the Built Environment*, vol. 22, no. 6, pp. 810–819, 2016.

[7] M. Hu, F. Xiao, and S. Wang, "Neighborhood-level coordination and negotiation techniques for managing demand-side flexibility in residential microgrids," *Renewable and Sustainable Energy Reviews*, vol. 135, p. 110 248, 2021.

[8] T. Jiang, Z. Li, X. Jin, H. Chen, X. Li, and Y. Mu, "Flexible operation of active distribution network using integrated smart buildings with heating, ventilation and air-conditioning systems," *Applied energy*, vol. 226, pp. 181–196, 2018.

[9] H. Fontenot, K. S. Ayyagari, B. Dong, N. Gatsis, and A. Taha, "Buildings-to-distribution-network integration for coordinated voltage regulation and building energy management via distributed resource flexibility," *Sustainable Cities and Society*, vol. 69, p. 102 832, 2021.

[10] Z. Zheng, J. Pan, G. Huang, and X. Luo, "A bottom-up intra-hour proactive scheduling of thermal appliances for household peak avoiding based on model predictive control," *Applied Energy*, vol. 323, p. 119 591, 2022.

[11] N. Lu and Y. Zhang, "Design considerations of a centralized load controller using thermostatically controlled appliances for continuous regulation reserves," *IEEE Transactions on Smart Grid*, vol. 4, no. 2, pp. 914–921, 2012.

[12] C. Jin, C. Yan, R. Tang, H. Cai, and R. Zeng, "A fast building demand response method based on supply–demand coordination for urgent responses to smart grids," *Science and Technology for the Built Environment*, vol. 25, no. 10, pp. 1494–1504, 2019.

[13] M. Song, W. Sun, M. Shahidehpour, M. Yan, and C. Gao, "Multi-time scale coordinated control and scheduling of inverter-based tcls with variable wind generation," *IEEE Transactions on Sustainable Energy*, vol. 12, no. 1, pp. 46–57, 2020.

[14] J. Vivian, E. Prataviera, F. Cunsolo, and M. Pau, "Demand side management of a pool of air source heat pumps for space heating and domestic hot water production in a residential district," *Energy Conversion and Management*, vol. 225, p. 113 457, 2020.

[15] C. Winstead, M. Bhandari, J. Nutaro, and T. Kuruganti, "Peak load reduction and load shaping in hvac and refrigeration systems in commercial buildings by using a novel lightweight dynamic priority-based control strategy," *Applied Energy*, vol. 277, p. 115 543, 2020.

[16] X. Wu, J. He, Y. Xu, J. Lu, N. Lu, and X. Wang, "Hierarchical control of residential hvac units for primary frequency regulation," *IEEE Transactions on Smart Grid*, vol. 9, no. 4, pp. 3844–3856, 2017.

[17] X. Hu and J. Nutaro, "A priority-based control strategy and performance bound for aggregated hvac-based load shaping," *IEEE Transactions on Smart Grid*, vol. 11, no. 5, pp. 4133–4143, 2020.

[18] X. Li, Z. Han, T. Zhao, J. Zhang, and D. Xue, "Modeling for indoor temperature prediction based on time-delay and elman neural network in air conditioning system," *Journal of Building Engineering*, vol. 33, p. 101 854, 2021.

[19] X. Kou, F. Li, J. Dong, *et al.*, "A scalable and distributed algorithm for managing residential demand response programs using alternating direction method of multipliers (admm)," *IEEE Transactions on Smart Grid*, vol. 11, no. 6, pp. 4871–4882, 2020.

[20] W. Li, S. Wang, and C. Koo, "A real-time optimal control strategy for multi-zone vav air-conditioning systems adopting a multi-agent based distributed optimization method," *Applied Energy*, vol. 287, p. 116 605, 2021.

[21] V. Khatana and M. V. Salapaka, "Dc-distadmm: Admm algorithm for constrained optimization over directed graphs," *IEEE Transactions on Automatic Control*, 2022.

[22] W. Jiang and T. Charalambous, "Distributed alternating direction method of multipliers using finite-time exact ratio consensus in digraphs," in *2021 European Control Conference (ECC)*, IEEE, 2021, pp. 2205–2212.

[23] K. Meng, Z. Y. Dong, Z. Xu, Y. Zheng, and D. J. Hill, "Coordinated dispatch of virtual energy storage systems in smart distribution networks for loading management," *IEEE Transactions on Systems, Man, and Cybernetics: Systems*, vol. 49, no. 4, pp. 776–786, 2017.

[24] D. Wang, C. S. Lai, X. Li, *et al.*, "Smart coordination of virtual energy storage systems for distribution network management," *International Journal of Electrical Power & Energy Systems*, vol. 129, p. 106 816, 2021.

[25] B. Wang, T. Zhang, X. Hu, Y. Bao, and H. Su, "Consensus control strategy of an inverter air conditioning group for renewable energy integration based on the demand response," *IET Renewable Power Generation*, vol. 12, no. 14, pp. 1633–1639, 2018.

[26] L. Tesfatsion and S. Battula, "Notes on the gridlab-d household equivalent thermal parameter model," 2020.

[27] M. Song, C. Gao, H. Yan, and J. Yang, "Thermal battery modeling of inverter air conditioning for demand response," *IEEE Transactions on Smart Grid*, vol. 9, no. 6, pp. 5522–5534, 2017.

[28] R. Tang, S. Wang, and C. Yan, "A direct load control strategy of centralized air-conditioning systems for building fast demand response to urgent requests of smart grids," *Automation in Construction*, vol. 87, pp. 74–83, 2018.

[29] S. Wang and R. Tang, "Supply-based feedback control strategy of air-conditioning systems for direct load control of buildings responding to urgent requests of smart grids," *Applied Energy*, vol. 201, pp. 419–432, 2017.

[30] M. Song, C. Gao, J. Yang, and H. Yan, "Energy storage modeling of inverter air conditioning for output optimizing of wind generation in the electricity market," *CSEE Journal of Power and Energy Systems*, vol. 4, no. 3, pp. 305–315, 2018.

[31] Y. Xu and W. Liu, "Novel multiagent based load restoration algorithm for microgrids," *IEEE Transactions on Smart Grid*, vol. 2, no. 1, pp. 152–161, 2011.

[32] M. Zeraati, M. E. H. Golshan, and J. M. Guerrero, "A consensus-based cooperative control of pev battery and pv active power curtailment for voltage regulation in distribution networks," *IEEE Transactions on Smart Grid*, vol. 10, no. 1, pp. 670–680, 2017.

[33] L. Xiao and S. Boyd, "Fast linear iterations for distributed averaging," *Systems & Control Letters*, vol. 53, no. 1, pp. 65–78, 2004.

[34] L. Y. Wang, C. Wang, G. Yin, and Y. Wang, "Weighted and constrained consensus for distributed power dispatch of scalable microgrids," *Asian Journal of Control*, vol. 17, no. 5, pp. 1725–1741, 2015.

[35] M. Zeraati, M. E. H. Golshan, and J. M. Guerrero, "Distributed control of battery energy storage systems for voltage regulation in distribution networks with high pv penetration," *IEEE Transactions on Smart Grid*, vol. 9, no. 4, pp. 3582–3593, 2016.

[36] A. Soukup, "Embedded Control Systems with Floating-Point DSCs," *Texas Instruments Incorporated, White Paper*, 2008.

[37] N. Bof, R. Carli, and L. Schenato, "On the performance of consensus based versus lagrangian based algorithms for quadratic cost functions," in *2016 European Control Conference (ECC)*, IEEE, 2016, pp. 160–165.

Zhuang Zheng (M'22) received the B.E. degree in Electrical Engineering and Automation from Zhejiang University, China, in 2017, and the Ph.D. in Architecture and Civil Engineering from City University of Hong Kong, in 2021. He is currently a Postdoctoral Research Fellow with the Department of Built Environment and Energy Engineering, The Hong Kong Polytechnic University. His research interests include smart energy management in power grid and built environment.

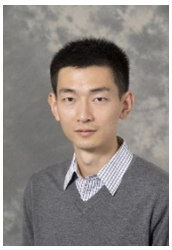

Rui Tang is a Lecturer in Smart Buildings and Digital Engineering at Institute for Environmental Design and Engineering, UCL, since February 2021. He conducts interdisciplinary works to facilitate the low-carbon technology transitions of multi-scale energy systems, spanning from building HVAC design and control, load prediction, demand response, and electricity pricing to large-scale modeling and data-driven techniques. Before joining UCL, he worked as a Senior Scientific Engineering Associate at Lawrence Berkeley National Laboratory (LBNL).

Xiaowei Luo received a B.Sc. degree in the Department of Civil Engineering from Tsinghua University in Beijing, China, in 2003, an M.S degree in Construction Management from Tsinghua University in 2006, and the Ph.D. degree in Construction Engineering and Project Management from the University of Texas at Austin in 2013. He is currently an Associate Professor in the Department of Architecture and Civil Engineering at the City University of Hong Kong. His main research interests include Building Information Modeling, Construction Safety Management, Information Technology in Construction, Wireless Sensor Technologies, and Green Building.

Hangxin Li is a research assistant professor in the Department of Building Environment and Energy Engineering at the Hong Kong Polytechnic University since March 2020. Before that, Dr. Li obtained her Bachelor's degree and Master's degree in Heating, Ventilation, and Air-conditioning Engineering from Hunan University in 2012 and 2015, respectively. Her Ph.D. was obtained in 2020 from the Hong Kong Polytechnic University. Her research expertise is mainly in zero/low energy buildings, uncertainty-based optimal design, optimal control of building energy systems, and building demand response.

Shengwei Wang received the BEng and MSc degrees in Refrigeration and Air-conditioning from Huazhong University of Science and Technology (HUST) in 1983 and 1986, respectively, and his Ph.D. degree in HVAC and Building Automation from the University of Liege in 1993. He is currently a chair professor and the director of the Research Institute for Smart Energy with The Hong Kong Polytechnic University. His research expertise and interests cover energy systems and building automation systems, energy-flexible buildings and demand response in smart grid, zero/low energy buildings, smart and distributed energy systems, cleanroom air-conditioning systems, district and data center cooling systems, uncertainty analysis in building and system design and control/diagnosis, next-generation key technologies for smart buildings.